

## Climatic Structure of the Dynamic and Temperature Fronts in the Scotia Sea and the Adjacent Water Areas

Yu. V. Artamonov , E. A. Skripaleva, N. V. Nikolsky

*Marine Hydrophysical Institute of RAS, Sevastopol, Russian Federation*

 [artam-ant@yandex.ru](mailto:artam-ant@yandex.ru)

### *Abstract*

**Purpose.** The aim of the work is to clarify the spatial structure of the climatic dynamic fronts (geostrophic current jets) and to estimate the relationship between their position and that of the large-scale temperature fronts on the surface of the Scotia Sea and the adjacent water areas in the southwestern part of the Atlantic sector of Antarctica.

**Methods and Results.** The daily averaged data arrays of the CMEMS (1993–2017) and NOAA OI SST (1982–2017) reanalysis at the regular 0.25° grid were used. The CMEMS reanalysis contains the sea surface geostrophic velocity values, the NOAA OI SST reanalysis – the sea surface temperature ones which were reduced to the climatic form through their averaging for each month of the corresponding periods. Position of the current jets and the temperature fronts was determined using the maximums of the geostrophic velocity components and the extremes of the temperature horizontal gradients. The updated scheme of the average long-term position of dynamic fronts was constructed. It shows that in the areas of the most pronounced bottom topography inhomogeneities (the northern boundary of the Falkland Plateau and the Tierra del Fuego shelf, the boundaries of the Falkland Islands shelf and the Birdwood Bank, the Shackleton Ridge and the South Shetland Islands shelf), the fronts do not change their latitudinal position during a year. It is revealed that in most of the water area, the temperature horizontal gradient extremes (temperature fronts) correspond to the geostrophic velocity maximums (dynamic fronts). The Northern and Central Branches of the Antarctic Circumpolar Current are most clearly manifested in the temperature field. In general, in the water area under study, the average annual latitudinal position of the Subantarctic and Antarctic Polar Fronts is displaced to the south relative to the position of the Northern and Central branches jets of the Antarctic Circumpolar Current by 0.25–0.5° and 0.25–1°, respectively.

**Conclusions.** It is shown that, being influenced by the bottom topography, the large-scale jets of geostrophic currents form intense topographic meanders and recirculation branches which are stably manifested on the climatic scale. The Antarctic Circumpolar Current branches being affected by the bottom topography, can merge forming the joint flows, and then diverge forming a system of separate jets again. It is found that the main spatial features of frontal structure in the geostrophic velocities field persist throughout the whole year and are conditioned mainly by the bottom topography. The most of the dynamic fronts are shown to be clearly pronounced in the temperature field on the surface during a year. A high level of linear correlation between the positions of temperature fronts and current jets was revealed; the correlation coefficient values are 0.6–0.97.

**Keywords:** Scotia Sea, Drake Passage, Weddell Sea, sea surface temperature, satellite altimetry, temperature horizontal gradients, geostrophic currents, bottom topography

**Acknowledgments:** the work was carried out within the framework of the state assignment of FSBSI FRC MHI No. 0555-2021-0004 "Fundamental studies of oceanological processes that determine state and evolution of marine environment under the influence of natural and anthropogenic factors based on the observation and modeling methods".

**For citation:** Artamonov, Yu.V., Skripaleva, E.A. and Nikolsky, N.V., 2022. Climatic Structure of the Dynamic and Temperature Fronts in the Scotia Sea and the Adjacent Water Areas. *Physical Oceanography*, 29(2), pp. 117-138. doi:10.22449/1573-160X-2022-2-117-138

DOI: 10.22449/1573-160X-2022-2-117-138

117

ISSN 1573-160X PHYSICAL OCEANOGRAPHY VOL. 29 ISS. 2 (2022)



The content is available under Creative Commons Attribution-NonCommercial 4.0 International (CC BY-NC 4.0) License

## Introduction

Study of the Southern Ocean frontal system associated with the Antarctic Circumpolar Current (ACC) branches is of great scientific and applied importance [1–7]. Large-scale anomalies of sea surface temperature (SST) are monitored in the ACC zone, propagating eastward and largely determining global climate changes in the ocean–atmosphere system [7–11]. Structure and intensity of these anomalies is determined by the variability of hydrological fronts. Oceanic fronts also affect the distribution of biogenic elements due to increased vertical exchange between deep and surface waters in front zones and “mixing barrier” effect for frontal jets, which prevents the exchange of characteristics through fronts [4, 7, 8, 12–16].

Despite significant progress in the study of the system of the Southern Ocean fronts and currents [1–8, 10–13, 17–30], a number of questions remain open. Even for such well-studied regions as the Drake Passage and Scotia Sea, there is still uncertainty in the number of ACC jets and their corresponding fronts. Thus, in works [1–3, 8], based on the data of contact hydrological measurements, in the Drake Passage and Scotia Sea, three main ACC jets (Northern, Central and Southern) and, three fronts, accordingly, – Subantarctic (SAF), Polar (PF) and the ACC Southern Front. In [3], in addition to these main fronts, the authors identified another front that is not associated with the ACC branches (dynamic fronts) and is determined only by thermohaline features, the southern boundary of the ACC. In [2], the southern boundary of the ACC in the Drake Passage and above the continental margin of the South Shetland Islands was called the Continental Waters Boundary (CWB), and in the Scotia Sea, the Scotia Sea Front (SSF). According to [8], in the Scotia Sea, the ACC southern boundary, also called the Secondary frontal zone, corresponds to the ACC southern branch, while the ACC southern front is not distinguished as a separate one.

Other works based on the data of actual measurements show that, depending on the measurement period, from four to eleven или from 4 to 11) ACC jets could be observed in the Drake Passage [22–26]. Based on relatively long time series of satellite altimetry data (1992–2007), WOCE transoceanic hydrological sections and Argo buoys, 9 jets and, accordingly, dynamic fronts were identified in the entire ACC circumpolar zone. Three jets were traced in the SAF zone, three in the PF zone, two in the ACC Southern Front zone, and one corresponded to the ACC southern boundary. At the same time, the authors note that the jets merge in the Drake Passage, forming several “superjets” [5, 6].

Estimates of the ACC “superjets” transport in the Drake Passage showed that the most intense are the Northern, Central and Southern branches of the ACC [22–25]. For example, in November 2011, the total transport of three jets of the Northern Branch, three jets of the Central and two jets of the Southern Branch of the ACC amounted to 57.7; 51.7 and 20.1 Sv, correspondingly [25]. There is a good

agreement between the transports obtained from the data of the acoustic Doppler current profiler LADCP and as a result of calculations by the dynamic method. Thus, in November 2007, the total transport of the three main branches of the ACC were, according to LADCP data, 14.0; 58.2 and 48.1 Sv; according to geostrophic calculations 13.9; 57.5 and 47.8 Sv [23].

According to the simulation data using the inverse box model, which assimilates the data of instrumental velocity measurements using LADCP and the hydrological data of hydrographic stations for March 18–April 21, 1999, it is shown that in the Scotia Sea, the transport volume is redistributed between the ACC jets [27]. For example, an increase in the eastward transport of the Subantarctic Front jet (Northern branch of the ACC) from  $31 \pm 7$  Sv to  $48 \pm 4$  Sv and the formation of topographic branches of the Polar Front jet (Central branch of the ACC) were noted.

In one of the most recent works [7], it is noted that there is still no unambiguous opinion about the number of the ACC system fronts, since it varies in time and space. Therefore, there is no consensus on the way the dynamic fronts (current cores) correlate in position with the temperature fronts on the surface, which are most accurately identified due to the large number of long-term satellite data series. A number of works have shown that zones of high SST gradients, reflecting the structure of fronts on the surface, can qualitatively coincide in position with zones of high gradients of dynamic heights (dynamic fronts), reflecting the integral effect of the entire water layer from the surface to the depth of the reference horizon [7, 18–21]. According to other works, some temperature fronts on the surface can be noticeably shifted relative to the position of the current cores [1, 4, 26, 28]. In [1], based on all historical data of on-board ship measurements for 1898–1986, it was noted that the SAF and the jet of Northern branch jet of the ACC practically coincide in position, and the Antarctic Polar Front (APF) is shifted by about  $1.5^\circ$  of latitude to the south relative to the jet of Central Branch of the ACC. Based on the data of the World Ocean Atlas and SST satellite measurements, it was found in [4] that in the southwestern Atlantic sector of the Antarctic, the position of the jets of the three ACC branches is shifted by about  $1\text{--}2^\circ$  of latitude relative to the position of the corresponding fronts in the SST field. Based on the HiGEM global climate model, it was shown in [28] that in the areas where the deep isotherms slope to the surface, the maximum SST gradients (temperature fronts) are located to the south of the maximum sea level gradients (dynamic fronts).

In general, the analysis of literature sources has shown that there are contradictions in determining the structure of dynamic and temperature fronts, being largely associated with the use of various types of data by different authors and the use of different methods for identifying fronts. In this work, based on modern reanalyses, in which all available data of contact and satellite measurements are interpolated into regular grids with the same step, the features of the climatic structure of dynamic fronts (geostrophic currents) are refined and their relationship with the position of temperature fronts on the surface in the southwestern Atlantic sector of the Antarctic is analyzed.

## Materials and Methods

The paper considers the part of the Atlantic sector of the Southern Ocean located south of 45°S, between 70° and 25°W. The General Bathymetric Chart of the Oceans (GEBCO) data ([http://www.gebco.net/data\\_and\\_products/gridded\\_bathymetry\\_data/](http://www.gebco.net/data_and_products/gridded_bathymetry_data/)) with a spatial resolution of 15 arc seconds in longitude and latitude were used to construct the bottom topography map (Fig. 1).

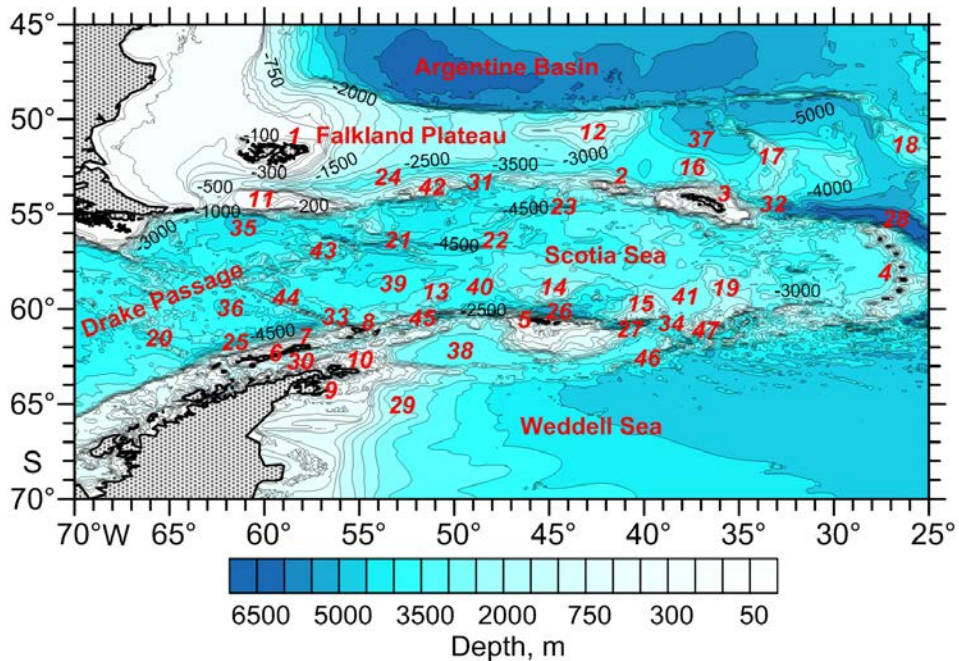


**Fig. 1.** Study area and bottom topography: 1 – Falkland Islands; 2 – Shag and Black Rocks; 3 – South Georgia Island; 4 – South Sandwich Islands; 5 – South Orkney Islands; 6 – South Shetland Islands; 7 – King George (Waterloo) Island; 8 – Mordvinov (Elephant) and Shishkov (Clarence) Islands; 9 – James Ross Island; 10 – Joinville Island; 11 – Burdwood Bank; 12 – Maurice Ewing Bank; 13 – Shackleton Bank; 14 – Pirie Bank; 15 – Bruce Bank; 16 – Northwest Georgia Rise; 17 – Northeast Georgia Rise; 18 – Islas-Orkadas Rise; 19 – Discovery Plateau; 20 – Hero Fracture Zone; 21 – Quest Fault; 22 – Endurance Fault; 23 – Tuelche Fault; 24 – Falkland (Malvinas) Trough; 25 – South Shetland Trench; 26 – South Orkney Trough; 27 – Orkney Trench; 28 – South Sandwich Trench; 29 – Aurora Canyon; 30 – Bransfield Strait; 31 – Shag Rocks Passage; 32 – Georgia Passage; 33 – Shackleton Passage; 34 – Bruce Passage; 35 – Yagan Basin; 36 – Phoenix Basin; 37 – Georgia Basin; 38 – Powell Basin; 39 – Ona Basin, 40 – Protector Basin, 41 – Scan Basin; 42 – North Scotia Ridge; 43 – West Scotia Ridge; 44 – Shackleton Ridge; 45 – South Scotia Ridge; 46 – Endurance Ridge; 47 – Bruce Ridge

Analysis of geostrophic circulation (dynamic fronts) was carried out using the array data from the Copernicus Marine Environment Monitoring Service (CMEMS) reanalysis ([http://marine.copernicus.eu/?option=com\\_csw&view=details&product\\_id=SEAL\\_EVEL\\_GLO\\_PHY\\_L4\\_REP\\_OBSERVATIONS\\_008\\_047](http://marine.copernicus.eu/?option=com_csw&view=details&product_id=SEAL_EVEL_GLO_PHY_L4_REP_OBSERVATIONS_008_047)). This array contains the daily average values of the zonal ( $U_g$ ) and meridional ( $V_g$ ) components of geostrophic velocity on the surface at the regular grid nodes with a step of 0.25° for 1993–2017, calculated as the sum of the mean dynamic topography according to the Aviso+ data (<http://www.aviso.altimetry.fr/en/data/products/auxiliary->

products/mdt) and daily average values of ocean level anomalies according to Jason-1, Jason-2, Jason-3, Sentinel-3A, HY-2A, Saral/AltiKa, Cryosat-2, TOPEX/Poseidon, ENVISAT, GFO and ERS1/2. Use of CMEMS reanalysis products for other World Ocean areas, in particular, for the Lofoten Basin [31] and the Arctic Ocean (AO) [32], showed good agreement between the results with the ORAS5 reanalysis [31] and the model of marine and oceanic circulation of the Institute of Numerical Mathematic Ocean Model (INMOM-Arctic), implemented for the Arctic Ocean and adjacent water areas [32]. In addition, in [32] it is noted that at present CMEMS is the most advanced operating system that provides data on the marine environment state of the entire World Ocean.

The frontal structure of the SST field was studied using the NOAA Optimum Interpolation Sea Surface Temperature (OI SST) reanalysis array ([https://psl.noaa.gov/cgi-bin/db\\_search/DBListFiles.pl?did=132&tid=89459&vid=2423](https://psl.noaa.gov/cgi-bin/db_search/DBListFiles.pl?did=132&tid=89459&vid=2423)). It contains daily average SST values at the regular grid nodes with a step of  $0.25^\circ$  for 1982–2017, obtained by the method of optimal interpolation of satellite and contact measurements, taking into account the sea ice concentration [33]. These arrays were selected due to three main reasons: firstly, the high spatial resolution allows to analyze the frontal structure in coastal areas and narrow straits; secondly, the same grid spacing permits to correctly compare the position of the cores of geostrophic currents and temperature fronts; thirdly, a data period of 25 or more years is sufficient to obtain statistically reliable climatic norms<sup>1</sup>. The daily average values of the geostrophic velocity and temperature components were reduced to the climatic form by averaging the time series of these parameters at each grid node, first for each month of each year, and then for the entire time period for each array (25 and 36 years). It resulted in smoothing out the synoptic and interannual variability of these characteristics. The days and months for which data were not available due to the presence of continuous ice cover (mainly in the Weddell Sea) were not taken into account in the averaging. Generally, the work analyzed areas where the seasonal ice concentration did not exceed 80 %, i. e., the ice-free water area within the  $0.25^\circ \times 0.25^\circ$  trapezium was over 20 %. Further, at each grid node, the magnitude of the velocity modulus and the current vector direction were calculated from the climatic values  $U_g$  and  $V_g$ , and the values of TMG (temperature meridional gradient), TZG (temperature zonal gradient), and TTG (temperature total gradient) were calculated from the SST values.

The spatial position of the dynamic and temperature frontal zones was analyzed from the distributions of the magnitudes of the velocity modules, vectors of geostrophic currents and the total horizontal SST gradient, respectively. When identifying temperature fronts, the criterion for the maximum (in absolute value) of the horizontal temperature gradient was used; when identifying the current (dynamic front) core, the criterion for the maximum gradient of the dynamic height (or maximum geostrophic velocity) was used. The latitudinal or longitude position of the maxima of SST gradients and geostrophic velocity was determined on the meridional and zonal samples TMG, TZG  $U_g$  and  $V_g$  with a discreteness of  $2.5^\circ$ .

---

<sup>1</sup> Monin, A.S., 1999. [*Hydrodynamics of the Atmosphere, Ocean and Earth Interiors*]. St. Petersburg: Gidrometeoizdat, 523 p. (in Russian).

The velocity maxima positions on the latitudinal and meridional profiles, together with the analysis of the spatial distribution of the velocity module and vector were used in constructing the general scheme of currents. When naming the branches of currents and temperature fronts, the nomenclature used earlier [4, 18, 19, 30] was applied; the name of the new branches of the currents, not described in the literature, was proposed by the authors of the present paper (table).

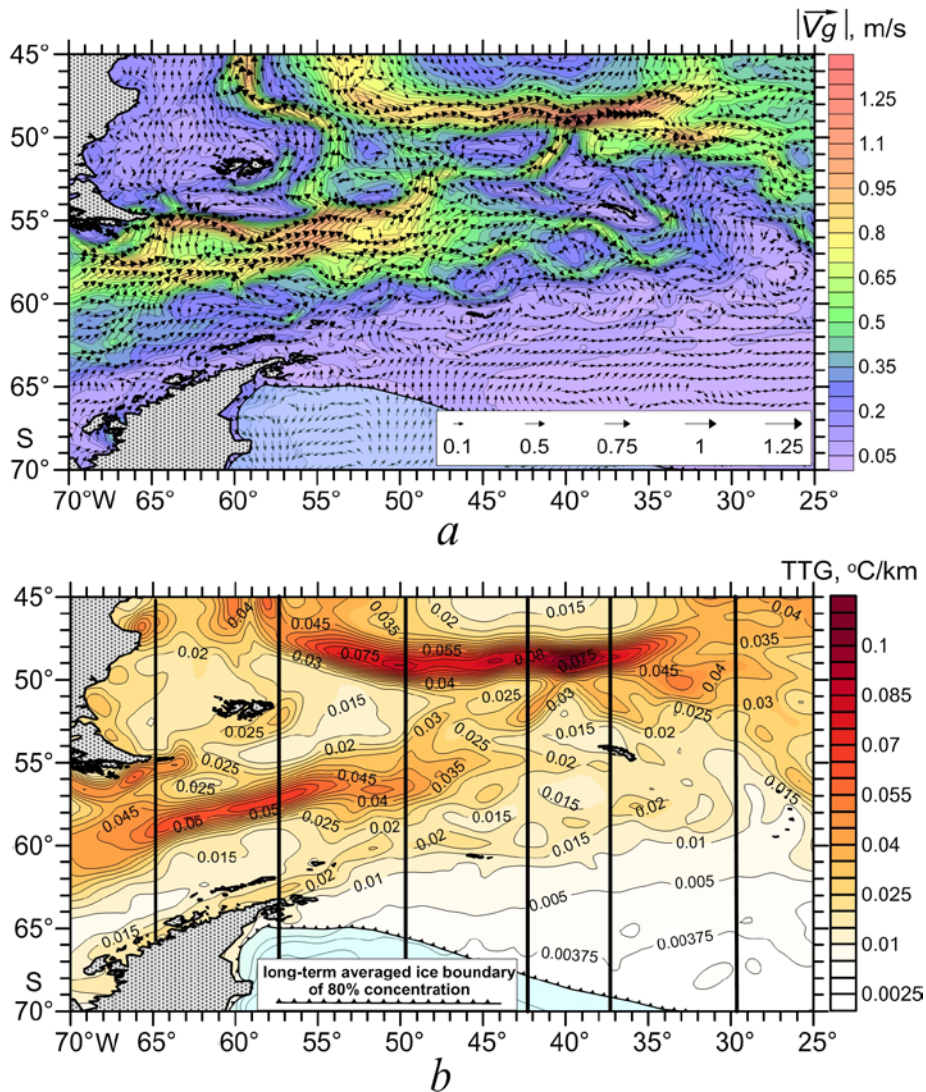
### Symbols for the names of currents and temperature fronts

Geostrophic currents (dynamic fronts)	
Antarctic Circumpolar Current	ACC
Jets of the Northern branch of the ACC	NB ACC, NB ACC-1, NB ACC-2
Jets of the Central branch of the ACC	CB ACC, CB ACC-1, CB ACC-2, CB ACC-3
Jets of the Southern branch of the ACC	SB ACC, SB ACC-1, SB ACC-2
Recirculations of jets of the Northern branch of the ACC	RNB ACC, RNB ACC-1
Recirculation of the Central branch of the ACC	RCB ACC
Recirculations of jets of the Southern branch of the ACC	RSB ACC, RSB ACC-1, RSB ACC-2, RSB ACC-3
Common stream of Northern and Central branches of the ACC	NB + CB ACC
Northern jet of recirculation of SB ACC-1	NRSB ACC-1
Southern jet of recirculation of SB ACC-1	SRSB ACC-1
Jets of Western Falkland Current	WFC, WFC-1
Eastern Falkland Current	EFC
Continental Water Boundary	CWB
Jets of Scotia Sea Front	SSF, SSF-1, SSF-2, SSF-3, SSF-4
Recirculation of Scotia Sea Front	RSSF
Jets of Weddell Gyre Boundary	WGB, WGB-1, WGB-2
Recirculation of WGB-1	RWGB-1
Common stream of SSF-1 and WGB	SSF-1 + WGB
Coastal current	CC
Northern periphery of the Bransfield Strait meander	NPBSM
Southern periphery of Bransfield Strait meander	SPBSM
Temperature fronts	
Subantarctic Front branches	SAF, SAF-2
Antarctic Polar Front	APF
Single frontal section formed by SAF and APF	SAF + APF
Branches of the Front of the Southern branch of the ACC	FSB ACC, FSB ACC-1
Coastal Shelf Front	CSF
Scotia Sea Front	SSF
Weddell Sea Front	WSF
Coastal front	CF

To assess the consistency of the temperature fronts' and current jets positions, the linear correlation between the spatial distributions of climatic average annual and monthly values  $|\vec{V}_g|$  and TTG,  $U_g$  and TMG along the meridians was analyzed. The statistical significance of the linear correlation coefficients was estimated at the 0.01 level, i. e., with 99 % confidence level.

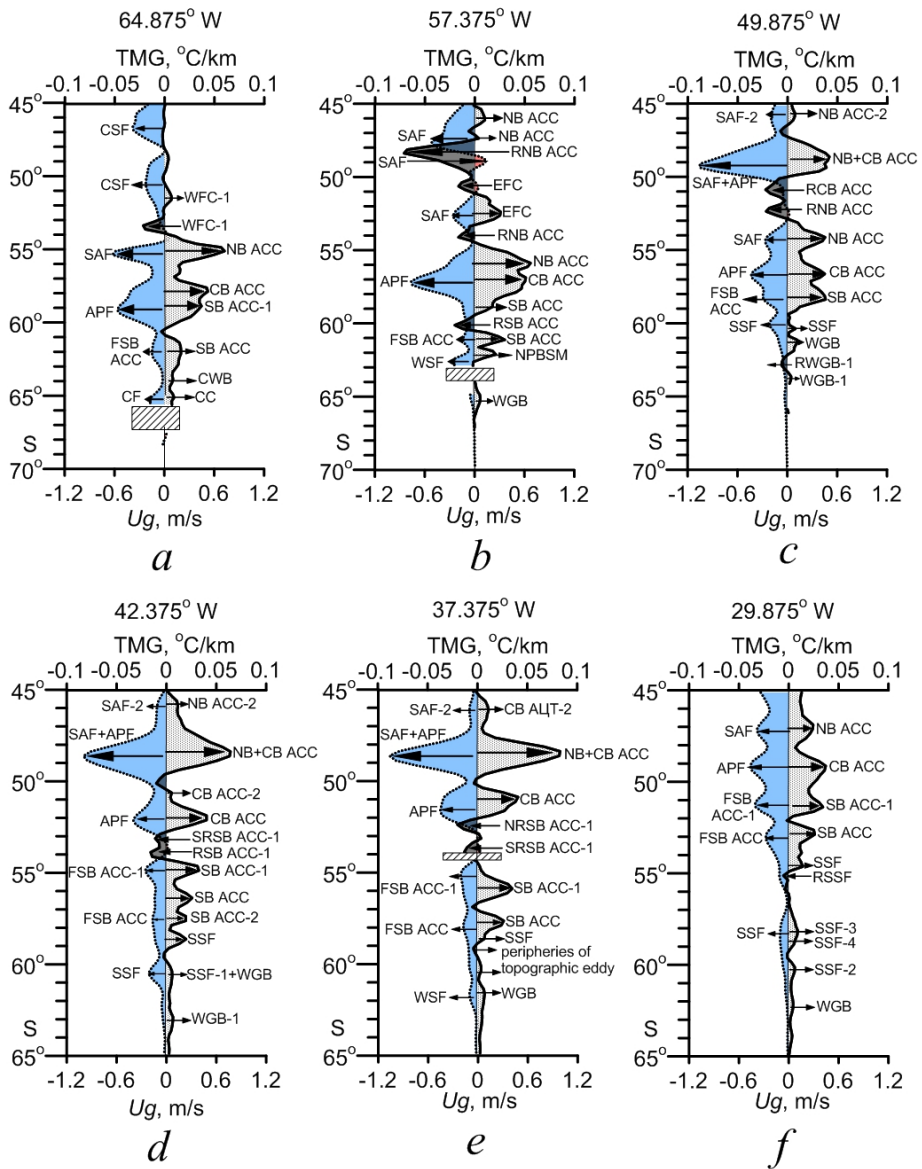
### The Study Results

The spatial distribution of the average annual vectors of geostrophic currents, their  $|\vec{V}_g|$  module (Fig. 2, *a*) and the average annual TTG values (Fig. 2, *b*) shows the presence of areas of increased values of these parameters. The identified areas are characterized by a rather complex structure and correspond to dynamic and temperature frontal zones, within which individual jets of currents with a maximum speed (dynamic fronts) and individual maxima of TTG values (temperature fronts) are traced, the number and position of which significantly change in space (Fig. 2).



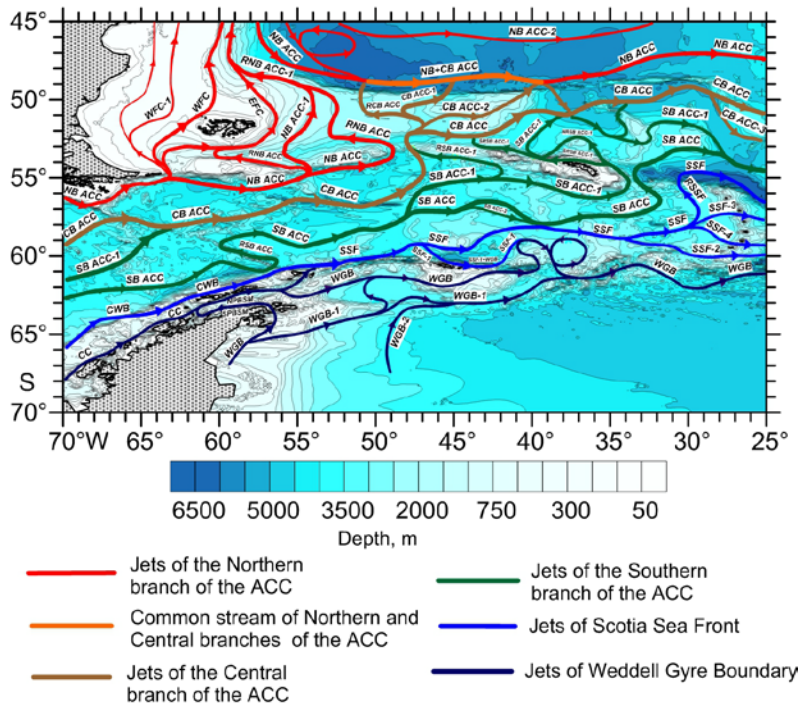
**Fig. 2.** Spatial distribution of the annual average climatic values: *a* – velocity module  $|v_g|$  and vectors of geostrophic currents; *b* – total temperature gradient (TTG) on the sea surface. Vertical lines show the meridians for which the annual average distributions of TMG and zonal velocity  $U_g$  are presented

Fig. 3 shows examples of the  $U_g$  and TMG latitudinal distributions along individual meridians. Their positions are shown in Fig. 2, *b*. In addition to the well-known main dynamic ACC system fronts, these distributions show less intense velocity maxima, associated either with the branches and meanders of the main currents, or with the peripheries of other dynamic formations (the Weddell Sea gyre, the cyclonic meander in the Bransfield Strait). Generally, there is a qualitative coincidence of the position of dynamic and temperature frontal zones (Fig. 2), the velocity maxima correspond to the extrema of the SST gradients (Fig. 3).



**Fig. 3.** Distribution of the climatic annual average TMG (dashed curves) and  $U_g$  (solid curves) values along 64.875°W (a), 57.375°W (b), 49.875°W (c), 42.375°W (d), 37.375°W (e), 29.875°W (f). Negative TMG values are shown in blue, positive ones – in red

A joint analysis of the spatial distributions of the vectors of geostrophic currents and the velocity module values (Fig. 2, a), the distributions of the average annual values of  $U_g$  and  $V_g$  along the meridians and parallels allowed to construct a refined scheme of the climatic position of the jets of geostrophic currents (Fig. 4). Their interpretation took into account the influence of bottom topography inhomogeneities (Fig. 1).



**Fig. 4.** Scheme of the average long-term position of the main geostrophic current jets against the background of bottom topography

The average annual climatic structure of dynamic and temperature fronts are considered below in accordance with their location from north to south. When mentioning one or another geographical object (islands, banks, ridges, straits, etc.), its numerical designation is given in brackets, shown in Fig. 1.

**Northern branch of the ACC (Subantarctic Front).** In the Drake Passage, the NB ACC jet runs along the shelf depths of Tierra del Fuego Island. (Fig. 4). The corresponding NB ACC in the temperature field, the Subantarctic Front, is located approximately 0.25° to the south (Fig. 3, a). To the east, part of the NB ACC waters penetrates to the north between Estados Island and Birdwood Bank (11) and goes around the Falkland Islands (1) in the form of the West Falkland Current, which consists of two main jets (WFC and WFC-1), and the more intense East Falkland Current (EFC) (Fig. 4). The other part of the NB ACC flow follows east over the Yagan Basin (35) to the south of Birdwood Bank. In the region of 54–55° Another part of the NB ACC waters penetrates to the north through a deep-water passage between the bank and the North Scotia Ridge (42) and is divided into two jets again. One jet turns to the west and passes along the northern boundary of the Birdwood Bank, forming the recirculation branch of the NB ACC (RNB ACC), which is in the region of 60°W merges with the EFC. Another jet (NB ACT-1) forms a cyclonic meander over the Malvinas Trough (24) and then follows north along an anticyclonic

trajectory over the continental shelf of the Patagonian shelf approximately along the 1,500 m isobath. Between 48° and 49°S. NB ACC-1 forms another recirculation branch (RNB ACC-1), which also merges with the EFC (Fig. 4). The main NB ACC jet continues eastward along the southern boundary of the North Scotia Ridge to approximately 49–50°W. Then it also turns to the north, passing over the western part of the deep water Shag Rocks Passage (31) and forms another recirculation branch of RNB ACC above the Malvinas Trough. This branch follows approximately along the 2,000 m isobath and north of 50°S merges with other NB ACC jets (Fig. 4). The recirculation branches of the RNB ACC and RNB ACC-1, the EFC quasi-zonal sections, and the main NB ACC jet along the southern boundary of the Birdwood Bank and the North Scotia Ridge are well traced on the meridional velocity profiles in the form of its extrema of different signs (Fig. 3, *b, c*). In the SST field, the Subantarctic Front is characterized by TMG extrema of different signs. To the north of the Falkland Islands, the SAF is characterized by positive gradients, since closer to the islands the average annual surface temperature is higher than the temperature of the waters transported from the south by the EFC. South of the Falkland Islands and to the east, near the southern boundary of the North Scotia Ridge, SAF is characterized by negative TMG and is observed south of NB ACC by about 0.5° (Fig. 3, *b, c*).

After the WFC, EFC and RNB ACC-1 merge, the NB ACC total stream follows north and approximately 40°S (outside the area under study) turns to the southeast, forming a cyclonic meander above the continental shelf of the Patagonian shelf [2, 4, 5]. Within the analyzed area, NB ACC is again traced to the east of 53°W in the form of a southeast direction stream, which consists of two main jets. At the western Argentine Basin boundary, approximately between 55° and 51°W, part of the NB ACC stream forms a closed anticyclonic gyre (Fig. 4). East of 52°W NB ACC follows the northern boundary of the Falkland Plateau, while in the area between 51° and 37°W the flow is noticeably enhanced due to the water supply of the CB ACC. According to [4], this common stream, is denoted by the abbreviation SW + CB ACC, and the corresponding front in the temperature field is SAF + APF. The NB + CB ACC stream along its entire length occupies a stable latitudinal position between 48° and 49°S, and the position of the SAF + APF temperature front is displaced to the south by about 0.5° (Fig. 3, *c – e*). East of 37°W the Northern and Central branches of ACC separate, while the NB ACC continues to follow the southern boundary of the Argentine Basin, gradually shifting northward to about 47°S (Fig. 3, *f*). In the SST field, SAF is located approximately 0.25° to the south (Fig. 3, *f*).

Note that north of the NB + CB ACC and NB ACC between 57° and 32°W a relatively weak stream, tentatively named NB ACC-2, can be found. It passes north of the deepest part of the Argentine Basin (Fig. 4). In the SST field, NB ACC-2 is manifested very weakly as a slight increase in TMG values (Fig. 3, *c – e*).

**Central branch of the ACC (Antarctic Polar Front).** In the Drake Passage, CB ACC follows a northeastern direction reaching approximately  $58^{\circ}\text{S}$  over the Shackleton Fault (Fig. 4). In the SST field, the Antarctic Polar Front corresponding to CB ACC is located here almost  $1^{\circ}$  south of the dynamic front (Fig. 3, *a*). To the east, CB ACC turns to the southeast, following the Shackleton Fault to about  $63^{\circ}\text{W}$  and further along the West Scotia Ridge (43), crosses the Quest Fault (21) and runs along the Endurance Fault (22) to about  $50^{\circ}\text{W}$  (Fig. 4). In this area, the APF is displaced by about  $0.5^{\circ}$  of the latitude to the south relative to the CB ACC jet (Fig. 3, *b, c*). East of  $50^{\circ}\text{W}$  CB ACC turns to the north and penetrates the Falkland Plateau through the eastern part of the deep water Shag Rocks Passage and the Malvinas Trough. Noticeable depth differences in the plateau area lead to the formation of several branches of the CB ACC, at least three of which merge with the NB ACC. One branch (recirculation branch) runs to the west at the southern boundary of the bottom elevation with depths of less than 2,300 m, goes around the elevation from the west and merges with the NB ACC at about  $51^{\circ}\text{W}$ . Another branch (CB ACC-1) passes over the deeper part of the Falkland Plateau to the west of the Maurice Ewing Bank (12) and in the region of  $45^{\circ}\text{W}$  merges with NB ACC. The third branch (CB ACC-2) runs along the southern boundary of the Maurice Ewing Bank over depths of 1000–1500 m and around  $40^{\circ}\text{E}$  approaches NB + CB ACC, then turns to the southeast (Fig. 3, *c*; 4), following along the western boundary of the Georgia Basin (37). Thus, the merge of the ACC Central Branch waters with the Northern Branch stream occurs not only to the east of the Maurice Ewing Bank, as noted earlier [2], but also to the west of it. The main part of the CB ACC stream passes south of the Maurice Ewing Bank over depths of 2,500–3,000 m, bends around it from the southeast and east of  $38^{\circ}\text{W}$  over the Georgia Basin merges with CB ACC-2 (Fig. 4). In this region, APF coincides in position with CB ACC (Fig. 3, *d*). Further, the CB ACC jet gradually shifts to the north and east of  $28^{\circ}\text{W}$  under the Islas-Orkadas Rise (18) influence, it is divided into two branches again – CB ACC-3 and CB ACC (Fig. 4). Here, the APF is traced approximately  $0.25$ – $0.5^{\circ}$  of latitude south of the CB ACC jet (Fig. 3, *e, f*).

**Southern branch of the ACC (Front of the Southern branch of the ACC).**

Two SB ACC jets are traced in the western part of the Drake Passage (Fig. 4). The northern jet (SB ACC-1) is oriented in a northeasterly direction; merges with CB ACC. The southern jet (SB ACC) crosses the Hero Fracture Zone (20) and follows the northern boundary of the South Shetland Trench (25) (Fig. 1, 4). In the SST field, the SB ACC core jet corresponds to the Front of the Southern branch of the ACC (FSB ACC) (Fig. 3, *a*). Then SB ACC follows through Shackleton Passage (33) and approximately between  $57$  and  $58^{\circ}\text{W}$  turns to the northwest along the Shackleton Ridge (44), forming the recirculation branch (RSB ACC). About  $60^{\circ}\text{W}$  this branch again turns to the east and follows the Ona Basin (39) (Fig. 4). The SB ACC meandering and recirculation appears on the meridional velocity profile as extrema of different signs (Fig. 3, *b*). Here, the FSB ACC in the SST field coincides

in position with the SB ACC jet (Fig. 3, *b*). Further, SB ACC passes north of the bottom elevation in the Shackleton Bank area (13) and over the northern part of the Protector Basin (40) (Fig. 4). Here, the FSB ACC temperature also well coincides in position with the SB ACC jet (Fig. 3, *c*).

In the central part of the Scotia Sea, SB ACC interacts with numerous inhomogeneities of the bottom topography, as a result of which it is characterized by an extremely complex spatial structure (Fig. 4). To the east about 48°W the SB ACC stream, following over depths of more than 3,500 m, is divided into two branches – SB ACC-1 and SB ACC. One branch (SB ACC-1) turns to the northeast, then passes south of the Tuelche Fault (23) and follows over depths of 3,500–4,000 m south of South Georgia Island (3). At the same time, about 42°W part of the SB ACC-1 waters turns to the west, following between the Tuelche Fault and the North Scotia Ridge, and forms a recirculation branch (RSB ACC-1), which is in the region of 47–48°W merges with CB ACC. Another part of the waters of SB ACC-1 passes south of South Georgia Island and, going around it from the east, forms two more recirculation branches to the north of it. One of them (Southern RSB ACC-1) follows west directly along the coast of South Georgia Island, and the other (Northern RSB ACC-1) goes around the Northwest Georgia Rise (16). In the region of 39–40°W these recirculation branches come close to each other. Then South RSB ACC-1 continues westward along the northern boundary of the North Scotia Ridge, passing north of Shag and Black Islands (2), and in the region of 43–44°W merges with CB ACC. The other branch (Northern RSB ACC-1) turns to the northeast and further, like SB ACC-1, between 38°W and 37°W close to CB ACC. Further, SB ACC-1 turns to the southeast and follows the southern periphery of the Georgia Basin, then, under the Northeast Georgia Rise (17) influence, splits into two streams again. Part of the water flows around the ridge from the northwest and merges with CB ACC, while the SB ACC-1 main flow goes around the ridge from the south and continues to follow the northern and eastern boundaries of the bottom elevation with depths of less than 3000 m (Fig. 4). On the whole, the existence of an anticyclonic turn of the SB ACC around the South Georgia Island, revealed in the present paper, according to the CMEMS reanalysis data, confirms the results of other authors. However, according to our study, the system of currents in the region of this island is characterized by a more complex structure than, for example, in [3, 27, 29].

After the SB ACC general stream division in two branches east of 48°W, the more southern SB ACC branch continues to follow east. Between 44° and 41°W it is also divided into two parts – SB ACC and SB ACC-2, passing over the 4000 and 3500 m isobaths, respectively. To the east, SB ACC goes around the bottom elevation with depths below 3000 m and shifts noticeably to the south. Between 33° and 31°W SB ACC forms an S-shaped meander, following through the Georgia Passage (32), then passes north of the South Sandwich Trench (28) approximately along the 3500 m isobath and east of 28°W merges with SB ACC-1 (Fig. 4).

Note that in the central and eastern parts of the Scotia Sea, the frontal structure of the SST field is noticeably simpler than the structure of the SB ACC flows. It is

characterized by two TMG extremes corresponding to the two main branches of the front (FSB ACC-1 and FSB ACC), while the recirculation branches of the SB ACC do not appear as temperature fronts (Fig. 3, *d – f*). In the central part of the water area, two FSB ACC branches practically coincide in position with the SB ACC-1 and SB ACC-2 jets (Fig. 3, *d*). To the east, at the South Georgia Island longitude, FSB ACC-1 is located almost  $1^\circ$  north of SB ACC-1 jet, and FSB ACC is displaced almost  $0.5^\circ$  south relative to SB ACC jet (Fig. 3, *e*). To the east of the Northeast Georgia Ridge, the FSB ACC-1 position coincides with the SB ACC-1 jet position, and FSB ACC is located almost  $0.5^\circ$  south of SB ACC (Fig. 3, *f*).

**Dynamic and temperature fronts of the southern part of the Drake Passage and the Scotia Sea.** In the southern part of the Drake Passage and the Scotia Sea south of SB ACC, relatively weak streams are observed (Fig. 2, *a*). According to existing concepts, there are two main fronts here: the Continental Waters Boundary and its continuation (the Scotia Sea Front), as well as the Weddell Gyre Boundary [2, 3, 30].

**Continental Waters Boundary and Scotia Sea Front.** An analysis of geostrophic current vectors and bottom topography (Fig. 1; 2, *a*) showed that the CWB corresponding stream passes over the continental Antarctic shelf and the shelf of the South Shetland Islands (Fig. 4). In the Drake Passage, in the long-term average temperature field on the CWB surface doesn't appear as a front (Fig. 3, *a*). To the east of King George Island (7), the CWB stream practically merges with the SB ACC (Fig. 3, *b*). To the east of Mordvinov Island (8) CWB, according to [2], is called the Scotia Sea Front and in the western part of the sea it runs along the northern boundary of the South Scotia Ridge (45) (Fig. 4). In this area, the temperature SSF can be traced almost  $0.5^\circ$  north of the dynamic front (Fig. 3, *c*). East of  $48^\circ\text{W}$  on the approach to the South Orkney Trough (26), the SSF splits into two branches, with the main branch passing over the continental slope to the south of the Pirie Bank (14), bending around it from the east. The other branch (SSF-1) the northern boundary of the South Orkney Islands shelf (5) follows and between  $42^\circ$  and  $43^\circ\text{W}$  it practically merges with the Weddell Gyre Boundary (WGB) (Fig. 4). The temperature SSF here coincides in position with the total SSF-1 + WGB flow jet (Fig. 3, *d*). East of  $42^\circ\text{W}$  approaching the Bruce Bank (15), the SSF-1 + WGB stream separates, while SSF-1 turns to the north, goes around the bank from the west and then merges with the WGB again (Fig. 4).

After rounding the Pirie Bank, the main SSF branch turns to the east, following over depths of 3000–3500 m, and in the region of  $40^\circ\text{W}$  to the south of the bottom elevation with depths less than 2500 m comes close to SB ACC. East of  $39^\circ\text{W}$  SB ACC and SSF diverge again, with the SSF shifting slightly to the south and passing north of the Discovery Plateau (19) at depths less than 2000 m (Fig. 4). In the SST field, SSF does not appear here (Fig. 3, *e*). East of  $34^\circ\text{W}$  the SSF stream is re-split into two branches. The southern weaker branch (SSF-2) continues to move

east-southeast along the northern boundary of the bottom elevation with depths of less than 2000 m and then passes south of the arc of the South Sandwich Islands (4). The main SSF stream follows to the northeast over depths of more than 3500 m and east of 30°E in turn is divided into three branches. One branch (the SSF itself) forms an S-shaped meander and bends around the island arc from the north, passing over the South Sandwich Trench (28). Two other branches (SSF-3 and SSF-4) follow in a quasi-zonal direction to the east through relatively deep water passages in the interisland zone (Fig. 4). Here, the temperature front is traced somewhat to the south of the SSF-3 core (Fig. 3, *f*).

Thus, the Continental Waters Boundary and its continuation, the Scotia Sea Front, are well traced in the long-term average field of geostrophic velocity as a separate dynamic front, which does not coincide with SB ACC in most of the water area. This result refines earlier ideas that the CWB and SSF are the southern boundary of the ACC, determined only by thermohaline features, but not identified as a dynamic front [3].

**The Weddell Gyre Boundary.** The Weddell Gyre Boundary (WGB), located south of the SSF, is a complex system of relatively weak currents, in which several branches can be distinguished. They form topographic meanders and gyres of various signs (Fig. 2, *a*).

Following along the eastern shelf of the Antarctic Peninsula, the WGB stream south of James Ross Island (9) is divided into two branches (Fig. 4). One part of the WGB waters penetrates through the Antarctic Strait into the Bransfield Strait (30) and forms the southern periphery of the cyclonic meander (SPBSM), the existence of which was noted earlier [8] (Fig. 4). It should be emphasized that the water inflow from the Weddell Sea into the Bransfield Strait, revealed from the CMEMS reanalysis data on the climatic time scale, was also observed from the data of individual hydrological surveys [8, 34–36]. Estimates of current costs in the Drake Passage based on the box model [27] also showed the existence of westward transport through the Bransfield Strait and along the Antarctic continental slope. The northern periphery of the cyclonic meander (NPBSM) is formed as a result of the confluence of the flow of the Weddell Sea waters, turning to the east, and the Coastal Current, penetrating into the strait from the west at 64°S (Fig. 4). In the SST field, the Coastal Current corresponds to a well-pronounced Coastal Front (Fig. 3, *a*). In the eastern part of the Bransfield Strait, the NPBSM stream is shifting northward to 62°S (Fig. 3, *b*) and approximately at the Joinville Island (10) longitude splits into two jets. One follows along the eastern trough of the Bransfield Strait, penetrates between the Mordvinov and Shishkov Islands (8) and merges with the SSF. Another jet is involved in the cyclonic circulation system of the Weddell Sea Gyre and follows east as WGB, passing over the northern shelf of the Joinville Archipelago and further over the northern part of the Powell Basin (38) (Fig. 3, *c*; 4). To the east, the WGB goes around the shallow part of the South Orkney Shelf with depths less than 500 m and between 42° and 43°E merges with SSF-1, forming a common

SSF-1 + WGB stream (Fig. 4). East of 41°E SSF-1 and WGB diverge, WGB passes along the southern boundary of the Orkney Basin (27), follows an S-shaped trajectory above the Bruce Bank, and slightly intensifies north of the bank due to re-merging with the SSF-1 flow. Then the WGB goes around the bank from the east, while part of the flow turns along an anticyclonic trajectory, forming a topographic eddy above the Skan Basin (41) (Fig. 3, *e*). The other part of the stream through the Bruce Pass penetrates south and east of 38°W merges with another WGB branch, called WGB-1. This branch is separated from the general WGB stream to the south of James Ross Island and follows northeast north of Aurora Canyon (29) (Fig. 4). Part of the WGB-1 flow goes around the eastern end of the Antarctic Shelf, penetrates into the Powell Basin and follows an S-shaped trajectory to the north, merging with the WGB (Fig. 3, *c*; 4). Another portion of WGB-1 waters follows the east along the southern boundary of the Powell Basin.

Between 49° and 48°W there is another quasi-meridional jet, WGB-2, which turns eastward at the Powell Basin boundary and merges with WGB-1 closer to the South Orkney shelf (Fig. 2, *a*; 4). Further, WGB-1 follows the southern boundary of the shelf, then gradually shifts to the north, passes along the northern boundary of the Endurance Ridge (46) and merges with the WGB (Fig. 3, *d*; 4). The general WGB flow follows eastward south of the Bruce Ridge and the elevation of the South Sandwich Islands arc bottom (Fig. 3, *f*; 4).

Note that the spatial structure of dynamic fronts in the WGB zone is noticeably more complex than the structure of temperature fronts on the Weddell Sea surface [30]. Corresponding to the WGB jet, the Weddell Sea front in the long-term average SST field is most clearly manifested in the eastern part of the Bransfield Strait (Fig. 3, *b*) and at the southern boundary of the Bruce Ridge (Fig. 3, *e*).

**Relationship between the spatial position of dynamic and temperature fronts.** An analysis of the average annual structure of the geostrophic velocity and surface temperature fields showed that in most cases, in the latitudinal range close to the position of the maximum velocity of a particular current, SST gradient extremum corresponding to the temperature front can be found. In the SST field the ACC branches in the form of the most intense Subantarctic and Antarctic Polar Fronts and the Front of the SB ACC are particularly clear. This is not entirely consistent with the results of [28], which states that SST gradients are inapplicable for detecting fronts in the Southern Ocean and studying the temporal variability of their position, since the gradients are too small in cold southern waters.

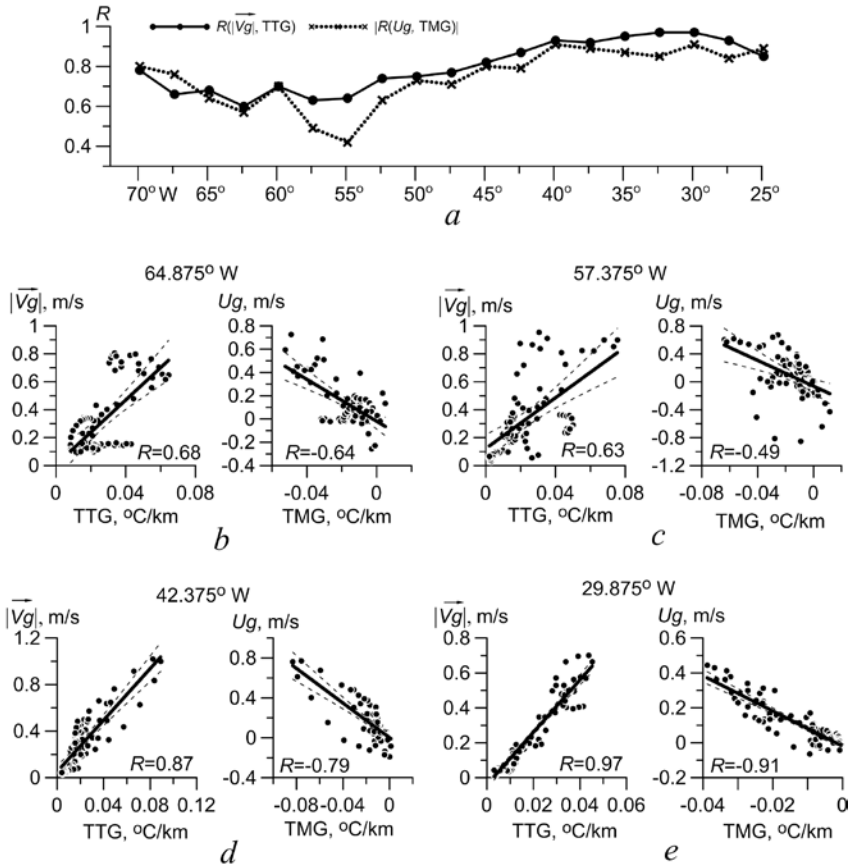


**Fig. 5.** Values of the linear correlation coefficients  $R$  between the average long-term distributions of the values of the geostrophic velocity module and the total temperature gradient  $R(|\vec{v}_g|, \text{TTG})$ , the zonal velocity and the temperature meridional gradient (in absolute value)  $|R(U_g, \text{TMG})|$  on individual meridians with discreteness  $2.5^\circ$  along the longitude (a); graphs of the linear correlation between the long-term average values of  $|\vec{v}_g|$  and TTG,  $U_g$  and TMG for the meridians  $64.875^\circ\text{W}$  (b),  $57.375^\circ\text{W}$  (c),  $42.375^\circ\text{W}$  (d),  $29.875^\circ\text{W}$  (e). Dashed lines denote the boundaries of the 99 % confidence intervals

Between the distributions of climatic average annual  $|\vec{v}_g|$  and TTG values,  $U_g$  and TMG along the meridians, a significant linear relationship was revealed at a 99 % confidence level, while the values of the correlation coefficients  $R$  between all parameters vary over space (Fig. 5). In the western part of the Drake Passage, they are 0.8 (in absolute value) (Fig. 5, a). To the east, on the meridians crossing the Drake Passage and the shallow part of the Patagonian shelf, the  $R$  values decrease and do not exceed 0.7 (Fig. 5, a, b). The decrease in the connection level is due to the fact that intense temperature fronts are observed over the shelf, and the currents are weakened (Fig. 3, a). In the range of  $60\text{--}55^\circ\text{W}$  the values of correlation coefficients  $R$  between  $|\vec{v}_g|$  and TTG are 0.65–0.7, between  $U_g$  and TMG 0.4–0.5 (Fig. 5, a, c). The decrease in the relation level of between  $U_g$  and TMG is due to

the fact that above the continental slope of the Patagonian shelf, an increase in the meridional velocity component and zonal gradients is observed, and intense zonal recirculation NB ACC branches are weakly manifested in the SST field (Fig. 3, *b*).

East of 55°W where the currents are more clearly manifested in the zonal velocity field, and the temperature fronts are predominantly quasi-zonal (Fig. 3, *c–f*), the values of the correlation coefficients  $R$  between all parameters increase and reach the highest values (above 0.8) east of 42°W (Fig. 5, *a, d*). The absolute maximum of  $R$  values (0.91–0.97) is observed in the region of 30°W (Fig. 5, *a, e*), where the best coincidence of the average annual position of the main dynamic and temperature fronts is observed (Fig. 3, *f*; 4).

The main features of the frontal structure in the fields of geostrophic velocities and temperatures persist from month to month. Fig. 6, *a, b* show examples of monthly average distributions of  $Ug$  and TMG values along the meridians crossing the western and eastern parts of the water area. It can be seen that all the main dynamic and temperature fronts are clearly traced during all months. The only exceptions are the southernmost fronts – the Coastal Current and the Coastal Front, the Scotia Sea Front branches in the eastern part of the water area, the Weddell Gyre Boundary and the Weddell Sea Front, which are not traced in the winter months of the Southern Hemisphere during the period of intense ice formation and the displacement of the ice boundary to the north (Fig. 6, *a, b*). In areas of the most pronounced inhomogeneities of the bottom topography (the northern boundary of the Falkland Plateau and the Tierra del Fuego shelf, the boundaries of the Falkland Islands shelf and the Birdwood Bank, the Shackleton Fault, and the continental shelf of the South Shetland Islands), the latitudinal position of the fronts practically does not change during the year. Thus, the spatial structure of fronts on the surface (their number and position) on the average annual and average monthly scales is determined mainly by the bottom topography, consistent with the results of model calculations [28].

The intra-annual variation of the linear correlation  $R$  coefficient values between the distributions of monthly averages and TTG (Fig. 6, *c*),  $Ug$  and TMG (Fig. 6, *d*) showed that in the western part of the water area there are noticeable changes in the level of linear relationship during the year. In the Southern Hemisphere (January–February) summer, the  $R$  values are minimal and do not exceed 0.2–0.45; in the period from late autumn to early spring, they increase and reach 0.7–0.8. This is due to the fact that significant intra-annual changes in the number, latitudinal position, and intensity of gradient extrema corresponding to coastal temperature fronts have been revealed on the Patagonian shelf. In the Southern Hemisphere summer, these fronts noticeably intensify, while the position and intensity of very weak dynamic fronts (meanders of the West Falkland Current) change insignificantly throughout the year (Fig. 6, *a*). To the east, the level of linear relationship between the distributions of monthly averages  $|\bar{v}_g|$  and TTG,  $Ug$  and TMG noticeably increases in all months, and east of 40°W  $R$  values remain within 0.85–0.97 throughout the year (Fig. 6, *c, d*).

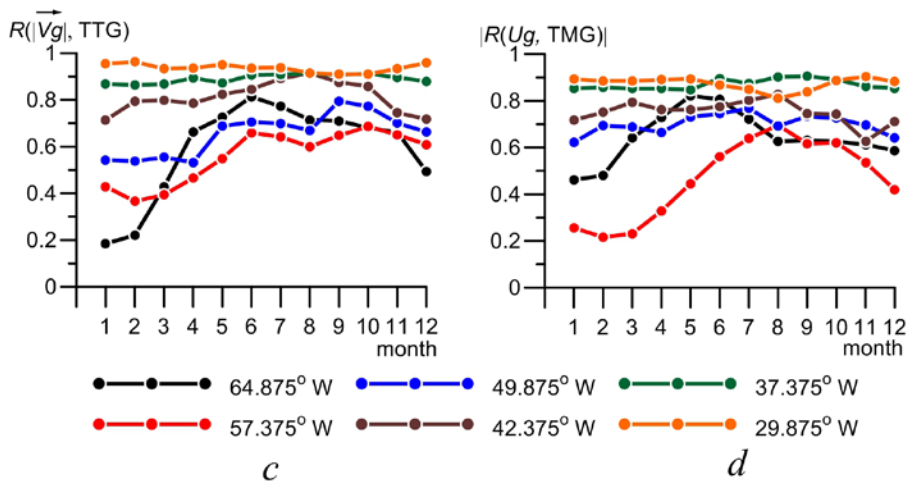
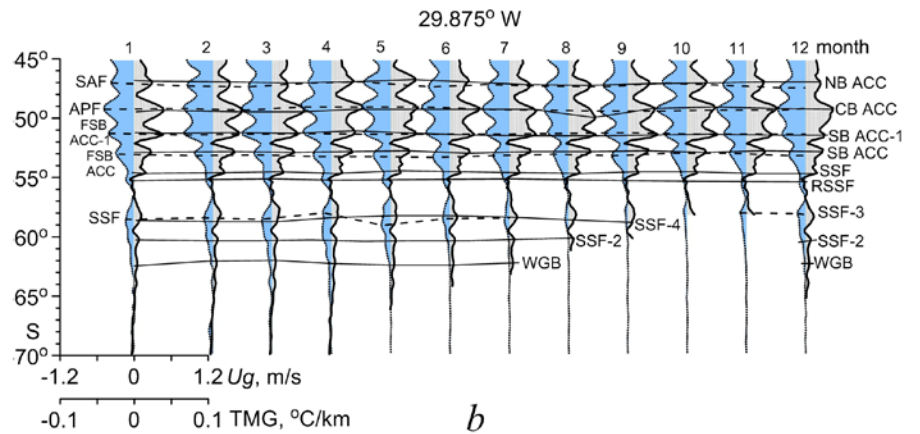
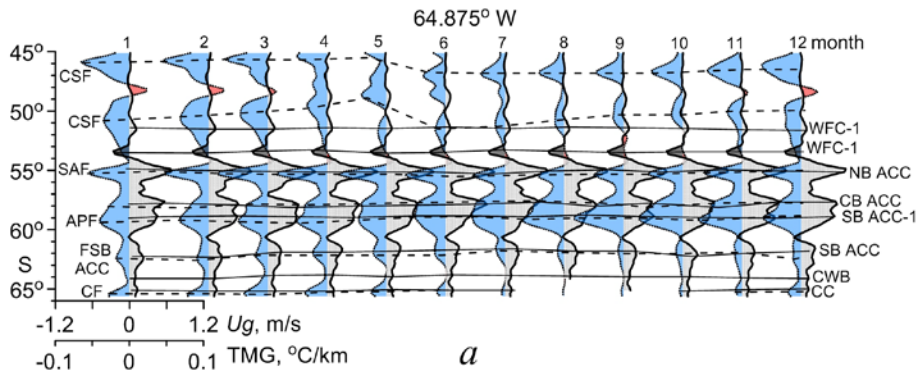


**Fig. 6.** Distribution of the climatic monthly average TMG (dashed curves) and  $U_g$  (solid curves) values along  $64.875^\circ\text{W}$  (a),  $29.87^\circ\text{W}$  (b); the intra-annual variation of the linear correlation coefficients  $R$  between the distributions of the monthly average values of  $|\vec{V}_g|$  and TTG (c),  $U_g$  and TMG (in absolute value) (d) for different meridians. Negative TMG values are shown in blue, positive ones – in red; solid lines denote positions of the current jets, dashed lines – positions of the temperature fronts

## Conclusion

Based on diurnal average data of the geostrophic velocity components of the CMEMS reanalysis, an updated scheme of the climatic position of the jets of geostrophic currents (dynamic fronts) on the surface of the southwestern Atlantic sector of the Antarctic is presented. It is shown that the long-term average structure of dynamic fronts is much more complicated than previously thought. The spatial position and number of dynamic fronts are related to the features of the bottom topography. Under their influence the fronts are divided into separate branches, meandering and the formation of recirculation branches. Intense topographic meanders and gyres of various signs, formed by dynamic fronts, are stably manifested on the climatic scale.

It is shown that, under the bottom topography influence, large-scale ACC branches can merge, forming common streams, and then diverge, forming a system of individual jets again. It has been established that the confluence of the waters of the Central Branch of the ACC with the Northern Branch current occurs not only to the east of the Maurice Ewing Bank, but also to the west of it. There, under the bottom topography influence, two more CB ACC branches are formed – the recirculating and CB ACC-1. It is revealed that the main features of the frontal structure in the field of geostrophic velocities (the number of branches of dynamic fronts and their position) are preserved from month to month. In areas where the fronts are influenced by the most pronounced bottom topography inhomogeneities (the northern boundary of the Falkland Plateau and the shelf of Tierra del Fuego, the boundaries of the Falkland Islands shelf and Birdwood Bank, the Shackleton Ridge, the continental shelf of the South Shetland Islands), they do not change latitude throughout the year.

It is demonstrated that in most cases dynamic fronts appear in the temperature field on the surface. In general, in the water area, the average annual position of SAF and APF in the SST field is shifted to the south relative to the position of the NB ACC and CB ACC jets by about  $0.25\text{--}0.5^\circ$  and  $0.25\text{--}1^\circ$  of latitude, respectively. A significant linear correlation has been established between the average annual position of dynamic and temperature fronts. The maximum level of relation (over 0.8 in absolute value) was found in the western part of the Drake Passage and east of  $42^\circ\text{W}$ . The absolute maximum of  $R$  values (0.91–0.97) is observed in the region of  $30^\circ\text{W}$ .

It is shown that in the western part of the water area, the level of relation between the position of dynamic and temperature fronts noticeably changes during the year. In the Southern Hemisphere summer, the  $R$  values are minimal and do not exceed 0.2–0.45; in the period from late autumn to early spring, they increase and reach 0.7–0.8. In the eastern part of the water area, the  $R$  values practically do not change during the year and remain within the range of 0.85–0.97.

## REFERENCES

1. Guretsky, V.V., 1987. Surface Thermal Fronts in the Atlantic Sector of the Southern Ocean. *Meteorologiya i Gidrologiya*, (8), pp. 81-89 (in Russian).
2. Peterson, R.G. and Stramma, L., 1991. Upper-Level Circulation in the South Atlantic Ocean. *Progress in Oceanography*, 26(1), pp. 1-73. doi:10.1016/0079-6611(91)90006-8
3. Orsi, A.H., Whitworth III, Th. and Nowlin Jr., W.D., 1995. On the Meridional Extent and Fronts of the Antarctic Circumpolar Current. *Deep Sea Research Part I: Oceanographic Research Papers*, 42(5), pp. 641-673. doi:10.1016/0967-0637(95)00021-W
4. Artamonov, Yu.V., Bulgakov, N.P., Lomakin, P.D., Skripaleva, E.A., Artamonov, A.Yu. and Stanichny, S.V., 2005. Structure and Seasonal Variability of Large-Scale Fronts in the Southwestern Atlantic and Adjacent Basins of the Antarctica Based on Hydrological and Satellite Data. *Oceanology*, 45(5), pp. 617-630.
5. Sokolov, S. and Rintoul, S.R., 2009. The Circumpolar Structure and Distribution of the Antarctic Circumpolar Current Fronts: 1. Mean Circumpolar Paths. *Journal of Geophysical Research: Oceans*, 114(C11), C11018. doi:10.1029/2008JC005108
6. Sokolov, S. and Rintoul, S.R., 2009. Circumpolar Structure and Distribution of the Antarctic Circumpolar Current Fronts: 2. Variability and Relationship to Sea Surface Height. *Journal of Geophysical Research: Oceans*, 114(C11), C11019. doi:10.1029/2008JC005248
7. Chapman, C.C., Lea, M.-A., Meyer, A., Sallée, J.-B. and Hindell, M., 2020. Defining Southern Ocean Fronts and Their Influence on Biological and Physical Processes in a Changing Climate. *Nature Climate Change*, 10, pp. 209-219. doi:10.1038/s41558-020-0705-4
8. Maslennikov, V.V., 2003. *Climatic Variability and Marine Ecosystem of the Antarctic*. Moscow: VNIRO Publishing, 295 p. (in Russian).
9. Turner, J., 2004. The El Niño – Southern Oscillation and Antarctica. *International Journal of Climatology*, 24(1), pp. 1-31. doi:10.1002/joc.965
10. Sallée, J.-B., Speer, K. and Morrow, R., 2008. Response of the Antarctic Circumpolar Current to Atmospheric Variability. *Journal of Climate*, 21(12), pp. 3020-3039. doi:10.1175/2007JCLI1702.1
11. Meredith, M.P., Murphy, E.J., Hawker, E.J., King, J.C. and Wallace, M.I., 2008. On the Interannual Variability of Ocean Temperatures around South Georgia, Southern Ocean: Forcing by El Niño/Southern Oscillation and the Southern Annular Mode. *Deep-Sea Research Part II: Topical Studies in Oceanography*, 55(18–19), pp. 2007-2022. doi:10.1016/j.dsr2.2008.05.020
12. Sokolov, S. and Rintoul, S.R., 2007. On the Relationship between Fronts of the Antarctic Circumpolar Current and Surface Chlorophyll Concentrations in the Southern Ocean. *Journal of Geophysical Research: Oceans*, 112(C7), C07030. doi:10.1029/2006JC004072
13. Venables, H., Meredith, M.P., Atkinson, A. and Ward, P., 2012. Fronts and Habitat Zones in the Scotia Sea. *Deep-Sea Research Part II: Topical Studies in Oceanography*, 59–60, pp. 14-24. doi:10.1016/j.dsr2.2011.08.012
14. Palter, J.B., Marinov, I., Sarmiento, J.L. and Gruber, N., 2013. Large-Scale, Persistent Nutrient Fronts of the World Ocean: Impacts on Biogeochemistry. In: D. Barceló and A. G. Kostianoy, 2013. *The Handbook of Environmental Chemistry*. Berlin, Heidelberg: Springer, pp. 1-38. doi:10.1007/978-3-642-24124-1\_241
15. Lohmann, R. and Belkin, I.M., 2014. Organic Pollutants and Ocean Fronts across the Atlantic Ocean: A Review. *Progress in Oceanography*, 128, pp. 172-184. doi:10.1016/j.pocean.2014.08.013
16. Nemirovskaya, I.A. and Kravchishina, M.D., 2016. Variability of Suspended Particulate Matter Concentrations and Organic Compounds in Frontal Zones of the Atlantic and Southern Oceans. *Oceanology*, 56(1), pp. 55-64. doi:10.1134/S0001437016010124

17. Patterson, S.L. and Sievers, H.A., 1980. The Weddell-Scotia Confluence. *Journal of Physical Oceanography*, 10(10), pp. 1584-1610. doi:10.1175/1520-0485(1980)010<1584:TWSC>2.0.CO;2
18. Artamonov, Yu.V. and Skripaleva, E.A., 2005. The Structure and Seasonal Variability of the Large-Scale Fronts in the Atlantic Ocean on the Basis of Satellite Data. *Issledovaniye Zemli iz Kosmosa*, (4), pp. 62-75 (in Russian).
19. Artamonov, Yu.V., Lomakin, P.D. and Skripaleva, E.A., 2008. Seasonal and Interannual Variability of the Characteristics of Scotia-Sea Front Based on the Satellite Measurements of Sea-Surface Temperature. *Physical Oceanography*, 18(1), pp. 52-62. doi:10.1007/s11110-008-9009-3
20. Artamonov, Yu.V. and Skripaleva, E.A., 2016. Oceanographic Research of Marine Hydrophysical Institute in the Southern Ocean. *Physical Oceanography*, (6), pp. 56-66. doi:10.22449/1573-160X-2016-6-56-66
21. Freeman, N.M., Lovenduski, N.S. and Gent, P.R., 2016. Temporal Variability in the Antarctic Polar Front (2002–2014). *Journal of Geophysical Research: Oceans*, 121(10), pp. 7263-7276. doi:10.1002/2016JC012145
22. Koshlyakov, M.N., Lisina, I.I., Morozov, E.G. and Tarakanov, R.Yu., 2007. Absolute Geostrophic Currents in the Drake Passage on the Basis of Observations in 2003 and 2005. *Oceanology*, 47(4), pp. 451-463. doi:10.1134/S0001437007040029
23. Gladyshev, S.V., Koshlyakov, M.N. and Tarakanov, R.Yu., 2008. Currents in the Drake Passage Based on Observations in 2007. *Oceanology*, 48(6), pp. 759-770. doi:10.1134/S0001437008060015
24. Koshlyakov, M.N., Gladyshev, S.V., Tarakanov, R.Yu. and Fedorov, D.A., 2011. Currents in the Western Drake Passage according to the Observations in January of 2010. *Oceanology*, 51(2), pp. 187-198. doi:10.1134/S000143701102007X
25. Koshlyakov, M.N., Gladyshev, S.V., Tarakanov, R.Yu. and Fedorov, D.A., 2013. Currents in the Drake Passage by the Observations in October–November of 2011. *Oceanology*, 53(1), pp. 1-12. doi:10.1134/S0001437013010062
26. Tarakanov, R. Yu. and Gritsenko, A.M., 2018. Jets of the Antarctic Circumpolar Current in the Drake Passage Based on Hydrographic Section Data. *Oceanology*, 58(4), pp. 503-516. doi:10.1134/S0001437018040100
27. Naveira Garabato, A.C., Stevens, D.P. and Heywood, K.J., 2003. Water Mass Conversion, Fluxes, and Mixing in the Scotia Sea Diagnosed by an Inverse Model. *Journal of Physical Oceanography*, 33(12), pp. 2565-2587. doi:10.1175/1520-0485(2003)033<2565:WMCFAM>2.0.CO;2
28. Graham, R.M., de Boer, A.M., Heywood, K.J., Chapman, M.R. and Stevens, D.P., 2012. Southern Ocean Fronts: Controlled by Wind or Topography? *Journal of Geophysical Research: Oceans*, 117(C8), C08018. doi:10.1029/2012JC007887
29. Thorpe, S.E., Heywood, K.J., Brandon, M.A. and Stevens, D.P., 2002. Variability of the Southern Antarctic Circumpolar Current Front North of South Georgia. *Journal of Marine Systems*, 37(1–3), pp. 87-105. doi:10.1016/S0924-7963(02)00197-5
30. Artamonov, Yu.V., Skripaleva, E.A. and Nikolsky, N.V., 2020. Spatial Structure and Intra-Annual Variability of Weddell Sea Front Based on the Data of NOAA OISST Reanalysis. *Ecological Safety of Coastal and Shelf Zones of Sea*, (4), pp. 89-102. doi:10.22449/2413-5577-2020-4-89-102 (in Russian).
31. Naumov, L.M. and Gordeeva, S.M., 2020. Lateral Heat and Salt Transports in the Lofoten Basin: Comparison Based on Three Databases. *Fundamentalnaya i Prikladnaya Gidrofizika*, 13(3), pp. 43-55. doi:10.7868/S207366732003003X (in Russian).

32. Fomin, V.V., Panasenkova, I.I., Gusev, A.V., Chaplygin, A.V. and Diansky, N.A., 2021. Operational Forecasting System for Arctic Ocean Using the Russian Marine Circulation Model INMOM-Arctic. *Arktika: Ekologiya i Ekonomika* [Arctic: Ecology and Economy], 11(2), pp. 205-218. doi:10.25283/2223-4594-2021-2-205-218 (in Russian).
33. Reynolds, R.W., Smith, T.M., Liu, C., Chelton, D.B., Casey, K.S. and Schlax, M.G., 2007. Daily High-Resolution-Blended Analyses for Sea Surface Temperature. *Journal of Climate*, 20(22), pp. 5473-5496. doi:10.1175/2007JCLI1824.1
34. Niller, P.P., Amos, A. and Hu, J.-H., 1991. Water Masses and 200 m Relative Geostrophic Circulation in the Western Bransfield Strait Region. *Deep Sea Research Part A: Oceanographic Research Papers*, 38(8-9), pp. 943-959. doi:10.1016/0198-0149(91)90091-S
35. Artamonov, Yu., Romanov, A., Vnucov, Yu., Perov, A. and Stepura, I., 2003. Results of the Oceanographical Research at the Western Bransfield Strait during March 2002. *Ukrainian Antarctic Journal*, (1), pp. 7-16 (in Russian).
36. Zhou, M., Zhu, Yi., Dorland, R.D. and Measures, C.I., 2010. Dynamics of the Current System in the Southern Drake Passage. *Deep-Sea Research Part I: Oceanographic Research Papers*, 57(9), pp. 1039-1048. doi:10.1016/j.dsr.2010.05.012

*About the authors:*

**Yuri V. Artamonov**, Leading Research Associate, Marine Hydrophysical Institute of RAS (2 Kapitanskaya St., Sevastopol, 299011, Russian Federation), Dr. Sci. (Geogr.), **ResearcherID: AAC-6651-2020**, artam-ant@yandex.ru

**Elena A. Skripaleva**, Senior Research Associate, Marine Hydrophysical Institute of RAS (2 Kapitanskaya St., Sevastopol, 299011, Russian Federation), Ph. D. (Geogr.), **ResearcherID: AAC-6648-2020**, sea-ant@yandex.ru

**Nikolay V. Nikolsky**, Junior Research Associate, Marine Hydrophysical Institute of RAS (2 Kapitanskaya St., Sevastopol, 299011, Russian Federation), **ResearcherID: AAC-7723-2020**, nikolsky.geo@gmail.com

*Contribution of the authors:*

**Yuri V. Artamonov** – general scientific supervision of the research, setting of study aims and objectives, qualitative analysis of the results and interpretation thereof, discussion of the study results, conclusions formulation

**Elena A. Skripaleva** – review of the literature on the research problem, qualitative analysis of the results and interpretation thereof, processing and description of the study results, discussion of the study results, conclusions formulation, article text preparation

**Nikolay V. Nikolsky** – development and debugging of computer programs for data processing and carrying out the necessary calculations, computer implementation of algorithms, graphs and diagrams construction, participation in the discussion of article materials

*The authors have read and approved the final manuscript.*

*The authors declare that they have no conflict of interest.*